Physical Science International Journal
9(3): 1-13, 2016, Article no.PSIJ.22868
ISSN: 2348-0130

SCIENCEDOMAIN *international*
www.sciencedomain.org

Spectrum Diagnostics of a Damaged Differential Planetary Gear during Various Operating Conditions

Xi Wu[1*], Andrew Sommer[2] and Jim Meagher[1]

[1]Department of Mechanical Engineering, California Polytechnic State University, San Luis Obispo, CA93407-0358, USA.
[2]Solar Turbines Incorporated, 9173 Sky Park Court, San Diego, CA92123-4341, USA.

Authors' contributions

This research is the joint effort of all authors. Author XW reviewed the research literature, proposed the idea how to proceed and gave the necessary training for ADAMS software. Author AS had done majority of the calculations and wrote the majority of the first draft of the manuscript. Author JM provided important ideas regarding spectrum diagnostics and modifications of the manuscript. All authors contributed and approved the final manuscript.

Article Information

DOI: 10.9734/PSIJ/2016/22868
Editor(s):
(1) Bheemappa Suresha, Department of ME, The National Institute of Engg, Mysore, India.
(2) Christian Brosseau, Distinguished Professor, Department of Physics, Université de Bretagne Occidentale, France.
Reviewers:
(1) Shao-Yi Hsia, Kao-Yuan University, Taiwan.
(2) Katarina Monkova, Technical University in Kosice, Slovakia.
(3) Lirong Wang, State University of New York at Stony Brook, USA.
(4) Piotr Czech, Silesian University of Technology, Poland.
Complete Peer review History: http://sciencedomain.org/review-history/12884

Original Research Article

Received 2nd November 2015
Accepted 22nd December 2015
Published 4th January 2016

ABSTRACT

Planetary gears are identified as compact alternatives to fixed-axis gear trains and show more complicated dynamical behavior due to the nonlinearity induced by the interaction between backlash and tooth defects. The majority of current publications are based on theoretical models of ideal planetary gears, and therefore cannot simulate the time varying dynamic forces induced by damaged teeth. By utilizing a multi-body dynamics and motion analysis software, this paper presents unpublished vibration spectra and fault indicators of a ubiquitous multi-input industrial differential planetary design that includes tooth damage. Backlash between the sun and planet gears are precisely dimensioned to avoid teeth interference and undercut. The region of point-to-point contact along the involute profile is modeled elastically and accounts for tooth flexibility. Boundary conditions that closely match realistic operation are considered, including component

**Corresponding author: E-mail: xwu@calpoly.edu;*

constraints, resistive bearing torques, and direct modification of the software parametric resolution. Torsional vibration induced by backlash and tooth geometry errors is shown to cause teeth separation and double-sided impacts in unloaded and lightly loaded gearing drives. Frequency analyses reveal distinct sideband modulations of the gear mesh along with sub and super harmonics. The sideband components, which comprise a large portion of the vibration, are used as fatigue diagnostics by identifying the location of manufacturing errors. Additionally, a joint time-frequency analysis (JTFA) is applied to transient start-up conditions that illustrates an oscillating spectrum in which contact forces increase during acceleration. To the best of our knowledge no research results have been published in fault detection of planetary gears using JTFA.

Keywords: Vibration health monitoring; malfunction diagnostics; contact forces; numerical simulation; planetary gear; epicyclic transmission; backlash; chipped tooth; multi-body kinematic model; joint time-frequency analysis.

1. INTRODUCTION

Planetary gears are widely used in industry from electrical screwdrivers to bulldozer power transmissions and automobiles. They can uniquely provide a lot of speed reductions and torques when weight and space v.s. reduction and torque are the biggest concern. A differential planetary gear is a specific type of planetary gear trains broadly used in automobiles and other wheeled vehicles. When the vehicle turns, the differential allows the outer wheel to rotate faster than the inner wheel.

Parker etc. [1-5] systematically explored the parametric instability of planetary gears while gear mesh stiffness is varying. They derived theoretical models and identified the main features of the natural frequencies and vibration modes of simple planetary gears. In addition to gyroscopic effects and time-varying gear mesh stiffness, they also integrated the practical factors of teeth separation, back-side contact, tooth wedging, and bearing clearances into their extended two-dimensional lumped-parameter models. Based on their successful theoretical models, they have made important conclusions about simple perfect planetary gears.

Unfortunately, majority of the current research and publications are based on theoretical models which cannot simulate the practical dynamic response of planetary gear train with damaged teeth. However, CAD and multi-body ADAMS software are useful tools to simulate the dynamic behavior of complicated planetary gears with backlash and damaged teeth. Kong and Meagher etc. [6] investigated the nonlinear contacts of a large gearbox, but did not consider backlash. Since the authors accurately design the gear profiles using CAD software and carefully choose simulation parameters in ADAMS, some interesting results of the dynamic forces are observed. ADAMS manual [7] provides some useful parameters for simulation. Sommer and Meagher etc. [8] illustrate the transient and steady state dynamic loading on teeth within a two-stage gear transmission arising from backlash and geometric manufacturing errors by utilizing a non-linear multi-body dynamics software model. Vibration and impact force distinctions between backlash and combinations of transmission errors are demonstrated under different initial velocities and load conditions. The backlash and manufacturing errors in the first stage of the gear train are distinct from those of the second stage. A joint time-frequency response analysis of the fixed-axis gears during start-up illustrates the manner in which contact forces increase during acceleration.

The lack of experimental results about the complicated dynamics of planetary gears and the availability of powerful multi-body dynamics software ADAMS inspire the authors to present this investigation. Some of our initial time-domain results about the differential gear have been published in the conference paper [9]. Based on our recent publications [8,9,11-16], we have extended and enhanced our research about the differential planetary gear by incorporating frequency analysis and JTFA in this paper.

(1). A practical differential planetary gear train with two inputs and one output is studied using multi-body dynamics software.
(2). Time domain results will show that the dynamic responses due to the combination of backlash and tooth defects depend on the interaction of many components of the differential planetary system.
(3). The non-linear factors such as periodically varying mesh stiffness due to alternating

tooth contact conditions, backlash, and tooth profile errors are all intrinsically incorporated into the ADAMS software. The dynamics of a differential planetary gear show a rich spectrum of nonlinear phenomena. Frequency analysis shows the appearance of side band modulations as well as harmonics of the gear mesh frequency.

(4). We will demonstrate how the frequency contents of the contact force evolve over time using a joint time-frequency analysis based on transient start-up conditions.

2. VALIDATING THE ADAMS MODEL USING PUBLISHED RESULTS

Due to lack of experimental data our multi-body kinematic model has been validated using the results from ASME Journal publication [10]. A pair of meshing gear parameters and ADAMS contact parameters are shown in Table 1. The gears are rigid with contact surfaces defined with a penalty based non-linear contact formulation. The non-linear contact force, $F = K(d)^e - cv$, is a vector quantity composed of an elastic and damping portion [77], where *d* is the penetration depth. The damping force, *cv*, is proportional to impact velocity, *v*. The selection of other parameters are described in detail in our paper [9].

Combined with gear profile errors backlash may cause loss of contact between gear teeth. This may induce consecutive single-sided or double-sided impacts and generate large impact forces with large vibration. R_p and R_g are the radii of the base circles of pinion and gear, respectively. θ_p and θ_g are the angular displacements of the pinion and gear, respectively. The relative displacement between the two mating teeth profiles along the line of action is represented as, $S = R_g\theta_g - R_p\theta_p$, shown in Fig. 1. When *S* is larger than the gear backlash *B*, there is contact between pinion and gear. For a fixed axis external spur pair,

$$-B \le R_g\theta_g - R_p\theta_p \le B$$

The results produced by the multi-body kinematic model are in very close agreement to the published results, shown in Fig. 2 and Fig. 3. More validation of our simulations are presented in our recent publication [11]. By making reasonable assumptions for these parameters, the ADAMS model has been validated for accuracy and robustness. This model accurately captures the dynamic forces and behavior of the mechanical transmission system and can be applied to the more complicated planetary gear.

Table 1. Geometric parameters and simulation contact force

Parameters		Value
Stiffness	*K*	1.8 x 10^5 Nmm
Force exponent	*e*	2.2
Damping	*c*	.27 Ns/mm
Penetration	d_c	1 x 10^{-3} mm
Elastic modulus	*E*	2.07 x 10^{11} Pa
Poisson's ratio	*v*	0.29
Density	*ρ*	7801 kg/m^3
Backlash	*B*	0.05 mm
Module	*m*	2 mm/tooth
Pressure Angle	*Φ*	20 deg
Face Width	*F*	10 mm
Pinion	Z_p	20 teeth
Gear	Z_g	80 teeth
Free vibration		50 rad/s pinion initial velocity
Constant torques		100 Nmm pinion torque -100 Nmm gear torque

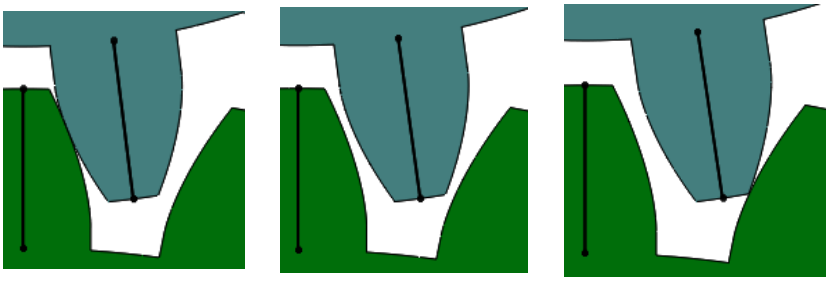

$R_g\theta_g - R_p\theta_p = -B$ $R_g\theta_g - R_p\theta_p = 0$ $R_g\theta_g - R_p\theta_p = B$

Fig. 1. Relative displacement along the line of action, $S = R_g\theta_g - R_p\theta_p$

3. MODELING A DIFFERENTIAL PLANETARY GEAR TRAIN WITH BACKLASH AND MISSING TEETH

The differential planetary gear chosen for study has two inputs and one output [11-13]. Some of the early preliminary research results of the authors had been published in references [14-16]. The system schematic and CAD model are shown in Fig. 4(a), and Fig. 4(b), respectively. The profile of the chipped sun gear tooth is shown in Fig. 5. Geometric design parameters of this planetary transmission are calculated in Table 2. The multi-body kinematic model formulation is defined in the same manner as in Section 1. Gear 1 driven by motor 2 is fixed-axis gear. It engages with the external teeth of the gear 2 which is part of the ring gear b. a driven by motor1 is the sun gear. c is the planet gear and *x* is the carrier.

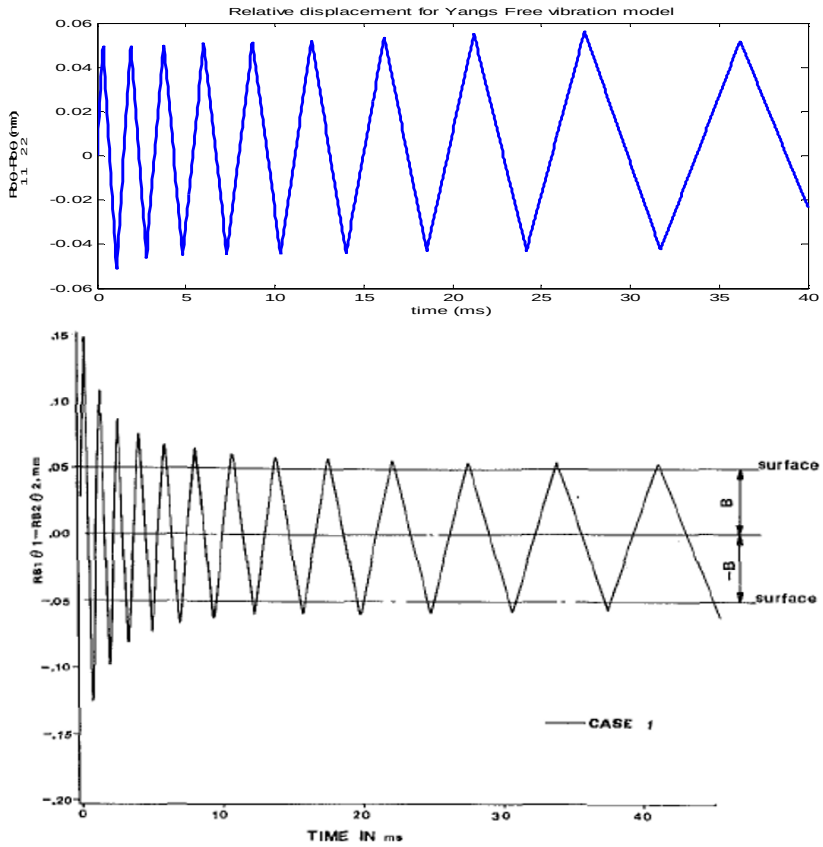

Fig. 2. Relative displacement comparison. Free vibration with 50 rad/s pinion initial velocity; Top: simulation result; Bottom: ASME Journal publication [10]

Table 2. Design and simulation parameters

Number of teeth	Z_a=20; Z_b = 94 Z_c= 37; Z_1 =28 Z_2 = 98	Material properties	E = 2.07 x 10^{11} Pa; v = 0.29; ρ = 7801 kg/m^3
Pitch diameter mm	D_a= 40; D_b = 188 D_c=74; D_1 =56 D_2 = 196	Force exponent	2.2
Module	2	Backlash	B_1 = 0.04 mm B_2 = 0.03 mm
Gearing ratios	5.7; 1.213	Penetration	10^{-7} mm
Pressure angle	20º	Stiffness	2 x 10^{7} N/mm

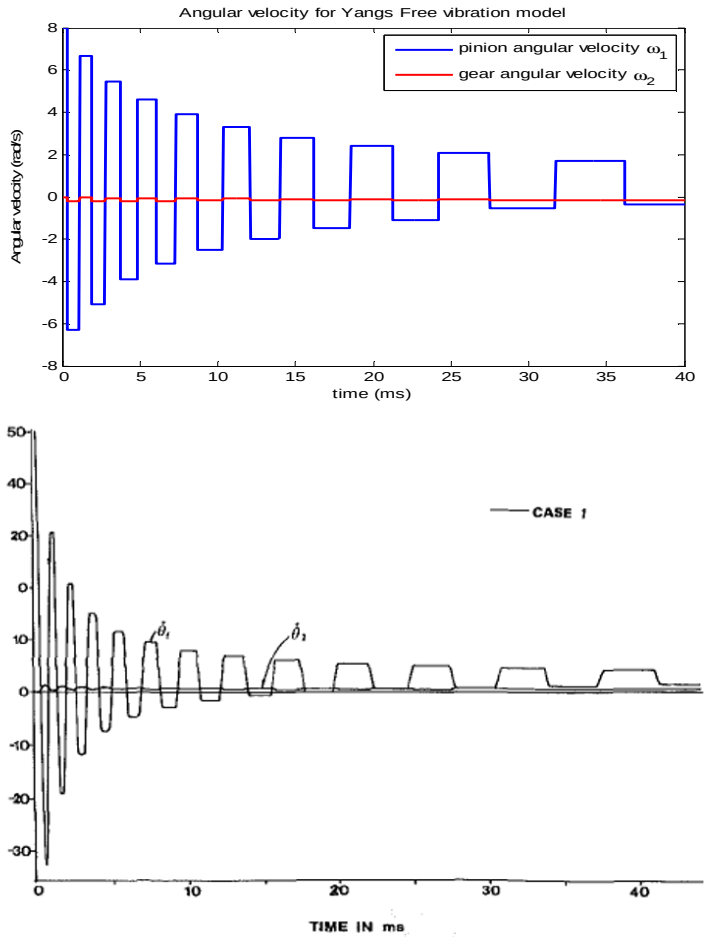

Fig. 3. Angular velocities comparison. Free vibration with 50 rad/s pinion initial velocity; Top: simulation result; Bottom: ASME Journal publication [10]

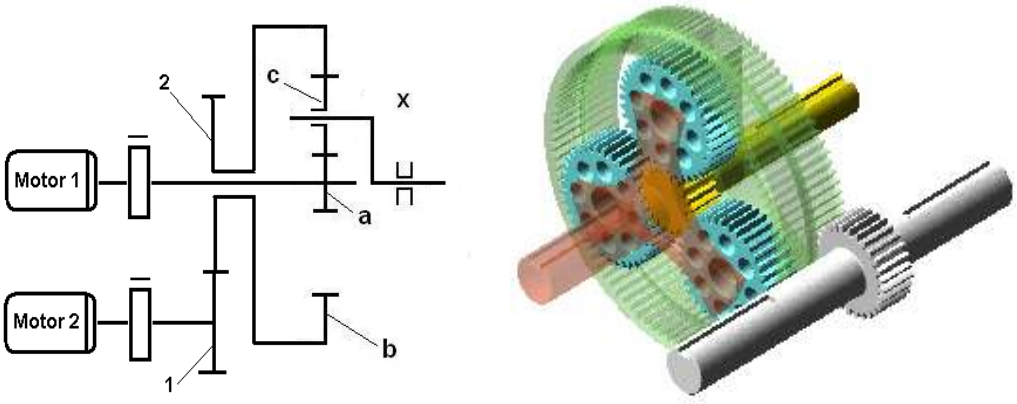

(a) Schematic **(b) CAD model**

Fig. 4. A differential planetary gear with two inputs and one output, the ring has both internal and external teeth

Fig. 5. Missing tooth profile

4. DYNAMIC RESPONSE AND DISCUSSION OF A PLANETARY GEAR WITH CONSTANT VELOCITY AND APPLIED STEP TORQUE TO THE SUN

The ring is held fixed and the sun is being driven by Motor 1 which has a constant angular speed of 102.1 rad/s = 975 rpm. The planet gears must be rotating in a direction opposite that of the sun and carrier for the engagement to be dynamically feasible. During the first few milliseconds the angular velocities change rapidly, then converge to an average speed consistent with their respective gearing ratios. The planet inertia is much smaller than the carrier assembly. Since the planets experience forces from the sun and internal ring, their angular velocities have a larger change in amplitude. These oscillations reduce quickly because the system is being driven by the kinematic constraint of a constant angular speed, which defines angular velocity ω as a function of time, ω = ω(t). Therefore, the sun will have the prescribed motion regardless of any force it experiences, causing the system to reach steady-state rapidly.

Consideration of a sun with a missing tooth is shown in Fig. 6. Between 1 and 3 ms the magnitude of the angular velocity has increased. This is because the planet has more room to move in the larger backlash induced by the damaged tooth. An impact force causes a change in angular acceleration which propagates further because of the profile gap. The response of the perfect involutes and chipped planets become nearly identical after 10 ms because the damaged tooth has moved through the engagement cycle.

With a fixed ring, a realistic step torque of the form $T(1-e^{t/\tau})$ is applied to the sun input shaft to represent an electric motor, with magnitude and time constant derived from rated operating conditions. The damaged sun experiences fewer impact events than the sun with standard involute profiles, shown in Fig. 7. It takes longer for the gears to contact due to the damaged tooth. The damaged sun experiences larger velocity changes because the torque has accelerated the sun for a longer time before contact. These velocity changes create large force magnitudes. The oscillations dissipate quickly as the system accelerates and contact between gear teeth becomes constant along one side only. Velocity changes from positive to negative, like those shown in Fig. 7, represent double-sided impacts induced by torsional vibration.

5. DYNAMIC RESPONSE AND DISCUSSION OF A PLANETARY GEAR WITH A STEP TORQUE APPLIED TO BOTH THE SUN AND GEAR 1

The system is operating in differential mode with Motor 1 and Motor 2 operating in the same direction. A step torque of the form $T(1-e^{t/\tau})$ is applied to both the sun and gear 1 to represent an electric motor, with the magnitude and time constant derived from rated operating conditions. With a fixed ring as in Fig. 8 (a), the sun exhibits the form of the step function used to model the input torque. The sun oscillates with the largest amplitude because it has the smallest inertia. The planets dissipate energy from the sun input to the carrier output. The three planets must accelerate the carrier's large inertia from rest. The amplitude of the sun's velocity change is reduced with the system operating as a differential transmission, shown in Fig. 8(b). Operating in the differential mode the ring and carrier move in the same direction as the applied torque on the sun. This makes the magnitude of the sun's angular velocity change more smooth compared to the simple planetary configuration with a fixed ring. The same effect is seen in the

other elements. The detrimental effects of the sun's chipped tooth are reduced with the system operating in the differential mode.

The mesh between gear 1 and ring has a smaller prescribed backlash than the sun and planet meshes. Therefore, contact occurs in this external fixed axis mesh before the sun and planets. A clear succession of impacts shown in Fig. 9. The interval from 3.5 ms to 4.5 ms shows that as gear 1 contacts the ring, the ring contacts a planet, and the planet contacts the sun. The planets can simultaneously be in contact with the sun and ring. This complication means that the force in the fixed axis mesh directly affect the magnitude of the force between a planet and ring, shown as the 10 N peak at 7.5 ms. The dynamic response of the planet is due to a superposition of the impacts in its sun and ring meshes.

6. STEADY-STATE FREQUENCY DOMAIN SIMULATION RESULTS AND DISCUSSION

The system is operating in the differential mode, with Motor 1 and Motor 2 operating in opposite directions. Constant angular velocities of 16.3 Hz = 975 rpm, and -12.4 Hz = 745 rpm, are applied to the sun and gear 1, respectively. A small resistive torque is applied to both the ring and carrier assembly. The value of the resistive torques are around one percent of the element's torque at steady-state. This resistive inertia models the frictional torque generated by the bearings, couplings, and fluid shear of the realistic planetary transmission. For testing purposes, a standard feedback control system can maintain the constant input speed on both shafts.

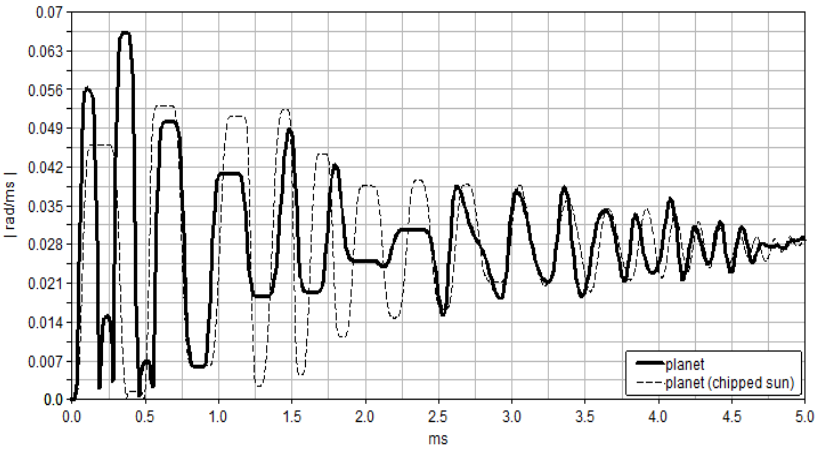

Fig. 6. Angular velocities when constant angular velocity ω_1 = 102.1 rad/s is applied to the sun

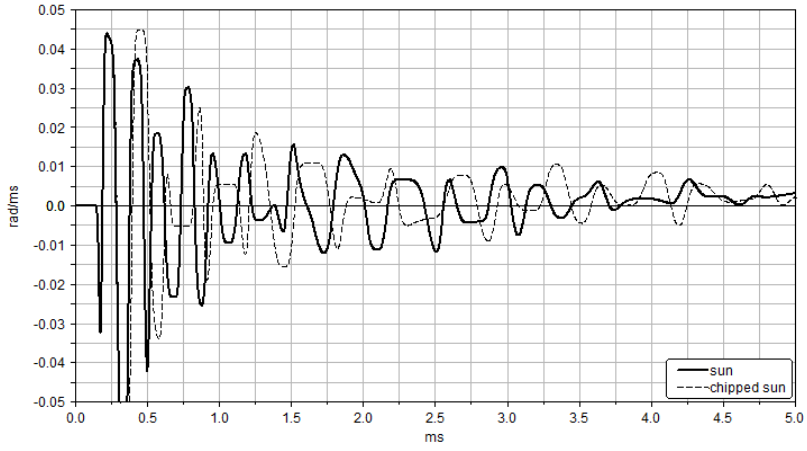

Fig. 7. Sun angular velocity when the torque T_1 = 70.5 Nm is applied to the sun

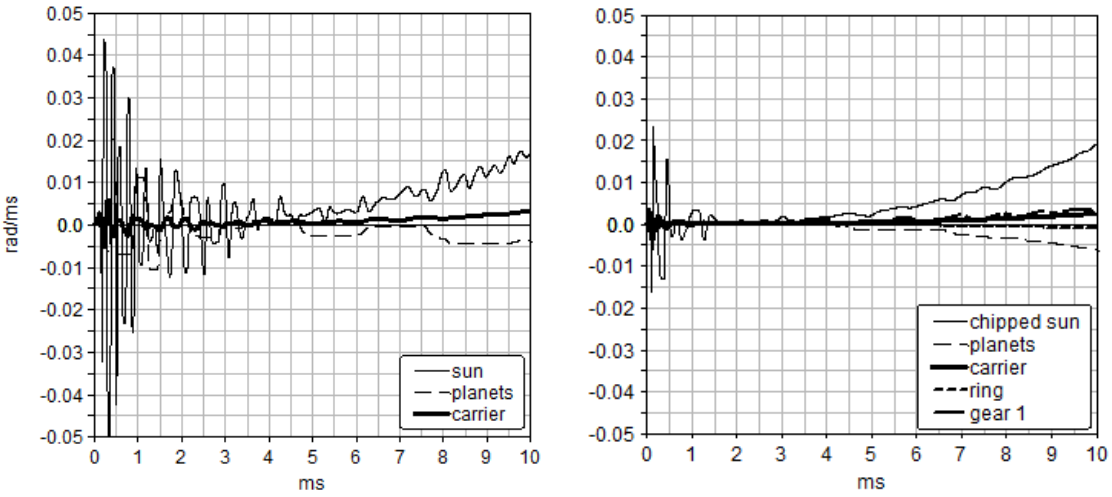

(a) Fixed ring, T_1 = 70.5 Nm **(b) Free ring, T_1 = 70.5 Nm, T_2 = 67.9 Nm**

Fig. 8. Angular velocity with applied step torques

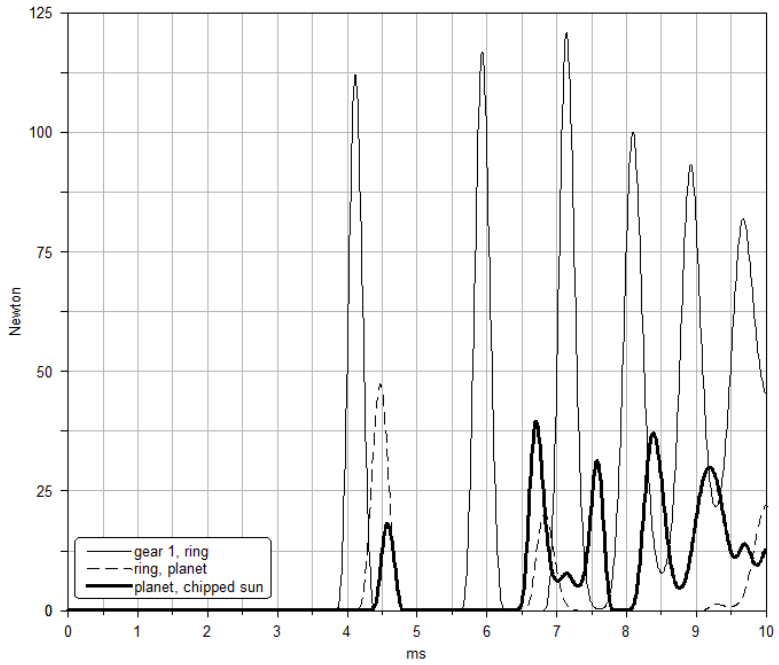

Fig. 9. Contact force when torque T_1 = 70.5 Nm is applied to the sun and T_2 = 67.9 Nm is applied to gear 1

The predicted spectrum includes harmonics of gear mesh frequencies and element spin speeds. Predicted frequencies up to 1000 Hz are calculated in Table 3. The sun, planet, and internal ring share the same *planetary* gear mesh frequency denoted as GMF_{abc}. The *fixed axis* mesh between gear 1 and the ring (gear 2) is denoted as GMF_{12}. This fixed axis mesh is characterized by a common factor of 14, therefore the n/CF subharmonics are included in the predicted spectrum. The *abc12* naming convention is consistent with the schematic of Fig. 4(a). Both the planetary and fixed axis meshes have unique force histories when the

transmission is operating in the differential mode, shown in Fig.10 for prescribed backlash and ideal involute profiles.

The fixed axis mesh between gear 1 and gear 2 is independent from the coupled kinematics of the planetary meshes. The largest amplitudes correspond to the gear meshing frequencies. The sidebands in the planetary mesh are modulations of sun spin speed because the sun is driven by Motor 1. Similarly, sidebands in the fixed axis mesh are modulated by the gear 1 spin speed because it is driven by Motor 2. The time and frequency domains of each mesh are shown in Fig. 10.

The planetary gear mesh frequency is modulated by the sun spin speed and its subharmonics, shown in Fig. 11. The sun spin speed subharmonics are a function of the number of planet gears calculated in Table 4. The subharmonics create wide 50 Hz sidebands around the gear mesh frequency. The fixed axis meshing frequency appears in the planetary mesh spectrum when a chipped tooth is included on the sun. The magnitude of the effect is reduced when an eccentric tooth is included on a planet. The fixed axis gear mesh frequency is modulated by the sun spin speed and its subharmonics although it is not included in the planetary mesh elements. The presence of GMF_{12} in the planetary mesh FFT indicates damage on a sun tooth. This is a potentially new and important vibration signature of the defected gear train.

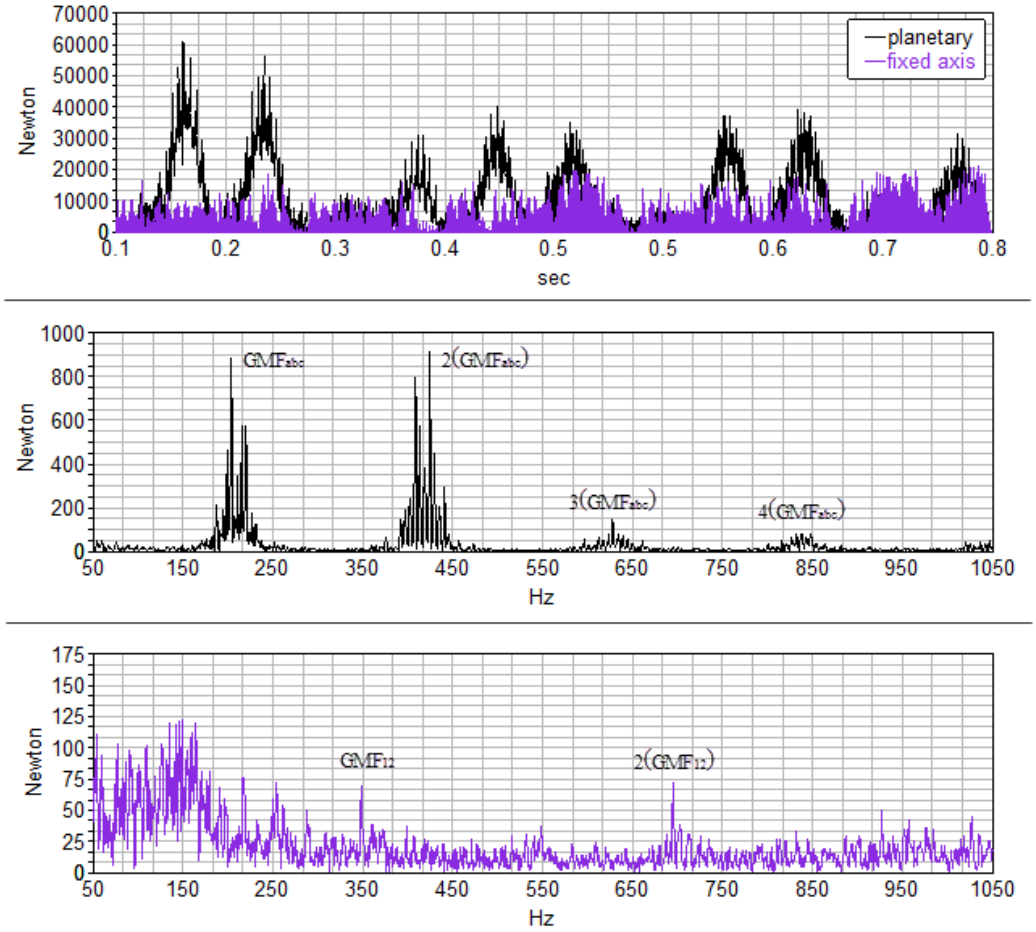

Fig. 10. Time and frequency domain representations of force in the planetary and fixed axis meshes

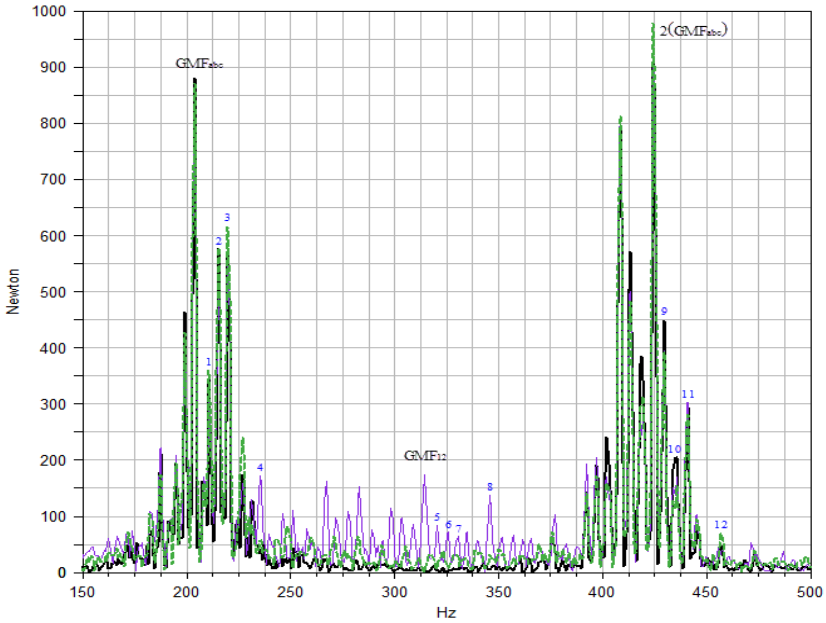

Fig. 11. Force magnitude in planetary mesh elements include modulated gear mesh frequencies

Table 3. Theoretical frequencies for the differential operating mode in Hz

	Frequency					Spin Speed		
	1X	**2X**	**3X**			**1X**	**2X**	**3X**
GMF_{abc}	209	419	628	Ring	f_r	3.6	7.1	10.7
GMF_{12}	347	695	1042	Carrier	f_c	5.8	11.6	17.3
1/14	25	50	74	Planet	f_p	6.1	12.3	18.4
2/14	50	99	149	Gear 1	f_1	12.4	24.8	37.2
3/14	74	149	223	Sun	f_s	16.3	32.5	48.8
4/14	99	199	298					
5/14	124	248	372					
6/14	149	298	447					
7/14	174	347	521					
8/14	199	397	596					
9/14	223	447	670					
10/14	248	496	745					
11/14	273	546	819					
12/14	298	596	894					
13/14	323	645	968					
1	347	695	1042					

7. JOINT TIME-FREQUENCY ANALYSIS (JTFA)

In order to demonstrate how the frequency content of force changes with time a joint time-frequency analysis (JTFA) is performed based on transient start-up conditions. Fig. 12 is created from the force history between gear 1 and the external teeth of the ring. The fixed axis force vector is chosen for study because of its unique interaction with the ring. The ring makes direct contact with all elements in the transmission except the sun. Therefore, the force vector between gear 1 and the ring contains information about the dynamics of the entire system. An exponential step of the form $\omega(1 - e^{t/\tau})$ is applied to both the sun and gear 1 to represent a characteristic electric motor. The magnitudes are -78.0 rad/s for gear 1, and 102.1 rad/s for the sun, with τ = 1000 ms. A resistive torque is applied to both the carrier assembly and the ring, with a magnitude around one percent of the

element's torque at steady-state. Aliasing issues are prevented by using a large number of integration steps and a long simulation duration of 4 seconds. Spectrum leakage is reduced by overlapping a sliding time sample of 100 ms by 98% and applying a Hamming window to each sample.

Table 4. Frequencies of Fig. 11

Sideband	Point	Hz
$GMF_{abc} \pm \frac{1}{3}f_s$	1	215
$GMF_{abc} \pm \frac{2}{3}f_s$	2	221
$GMF_{abc} \pm f_s$	3	226
$GMF_{abc} \pm 2f_s$	4	242
$GMF_{12} \pm \frac{1}{3}f_s$	5	352
$GMF_{12} \pm \frac{2}{3}f_s$	6	358
$GMF_{12} \pm f_s$	7	363
$GMF_{12} \pm 2f_s$	8	380
$2(GMF_{abc}) \pm \frac{1}{3}f_s$	9	424
$2(GMF_{abc}) \pm \frac{2}{3}f_s$	10	430
$2(GMF_{abc}) \pm f_s$	11	435
$2(GMF_{abc}) \pm 2f_s$	12	451

Due to the nonlinearity caused by the interaction of the damaged tooth and different backlash, a large number of contact events are created which occur at nearly random intervals. The random nature of the impacts produces a frequency domain with some noise. The low amplitude peaks observed between 1250 Hz and 1450 Hz continue until approximately 5000 Hz, with frequencies greater than 5000 Hz near zero. At 760 ms the second harmonic of the *fixed axis* gear mesh GMF_{12} is identified as the largest peak at 650 Hz. This value is less than the 695 Hz listed in Table 3 because the system has not accelerated to its full operating speed at τ = 1000 ms. The 3X(sun) speed is a strong excitation because of the chipped sun tooth. The damaged tooth rotates through a planet mesh three times per revolution. Therefore, the 3X(sun) speed is not a harmonic but rather the fundamental excitation of the chipped sun. The four largest peaks along the 760 ms line are modulated by the 3X(sun) frequency. The second harmonic of $2(GMF_{12})$ dominates the spectrum through the 650 to 1000 ms range with sidebands also equal to 3X(sun). The sidebands increase in frequency along with system speed to their final value of 48.8 Hz at 1000 ms. An increase in the separation between peaks is observed. Along the 1000 ms line the third harmonic of $3(GMF_{12})$ = 1042 Hz is present with sidebands of 3X(sun). The fourth harmonic of $4(GMF_{abc})$ = 838 Hz falls in this region with magnitudes comparable to the GMF_{12} harmonics. It notable that the fundamental GMF_{12}, GMF_{abc}, and $2(GMF_{abc})$ are not the dominant frequencies during start-up.

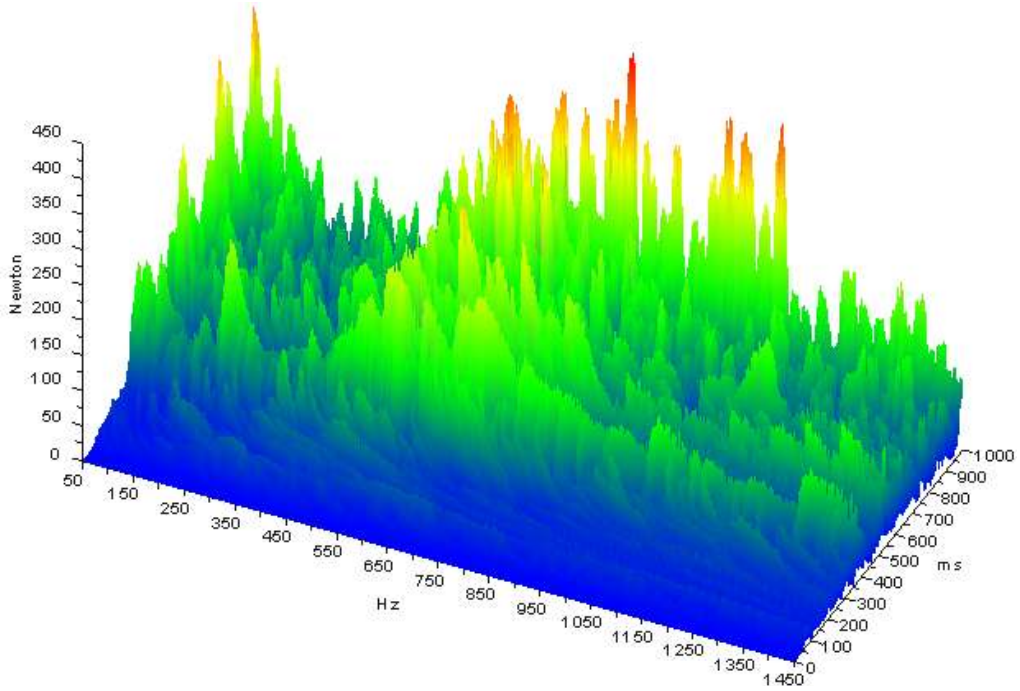

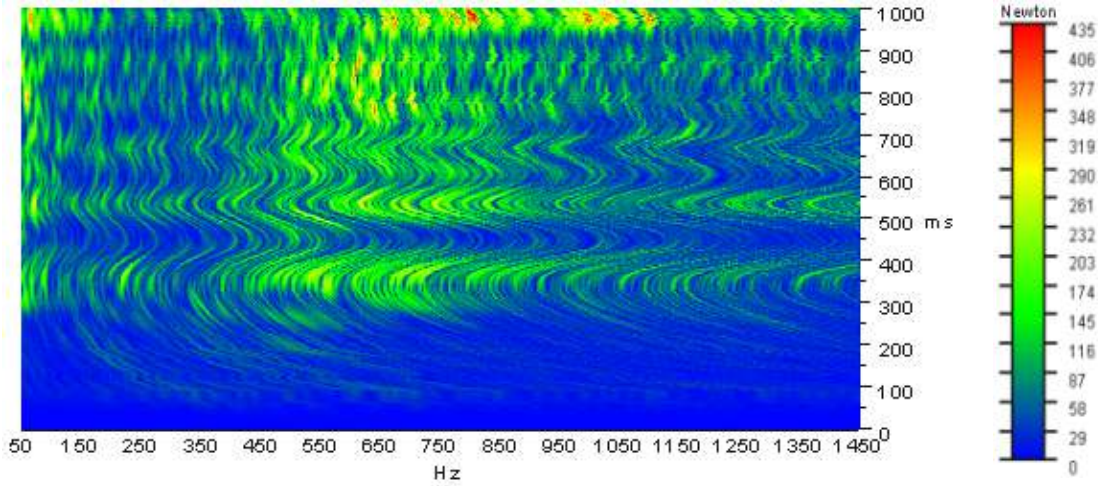

Fig. 12. Three dimensional FFT of force magnitude in the fixed axis mesh for prescribed backlash and chipped sun with an exponential step angular velocity on both sun and gear 1

The curvature in the spectral lines in the time domain is due to the acceleration of the ring. As the system accelerates from rest, the first contacts occur from gear 1 to the ring, and from the sun to each planet. The ring and planets oscillate within their backlash at high frequency because velocity is not prescribed on these elements. The ring accelerates away from the direction of contact up to 350 Hz, causing the contacts with gear 1 and the planets to occur at increasingly longer intervals. The ring's acceleration away from the direction of contact causes the frequency of all spectral lines to decrease. The opposite occurs during the interval of 350 ms to 450 ms. Here the ring decelerates slightly, decreasing the interval between contacts and causing an increase in spectral frequency. The magnitude of oscillation in the ring's acceleration diminishes with time with all spectral lines remaining straight for $t > \tau$.

8. CONCLUSIONS

This study compares the vibration spectra and transient kinetics of a multi-input industrial differential planetary design that includes tooth damage and backlash. A non-linear multi-body dynamics model of an ideal set of gears is first verified by comparison to published results. The model is then extended to include tooth profile errors are for comparison to ideal gears. The nonlinear contact mechanics model of the meshing teeth is built by careful calculation and selection of the contact simulation parameters such as the stiffness, force exponent, and damping and friction coefficients. The main conclusions from our research are:

(1). When the transmission operates with a fixed ring and undergoes free vibration from a near symmetrical position, six contact forces are potentially active. The magnitude of the contact forces depend on the time varying contact ratios of each element. The duration of the contact event decreases with a freely rotating ring and applied initial velocity.

(2). Step torques of opposite directions to each input shaft closely model the constraints and loading conditions of realistic operation. The dynamics of the differential mode are shown to be less destructive to the sun. The characteristics observed in the time and frequency domains are due to the interaction of many components of the differential planetary transmission.

(3). Fast Fourier Transform (FFT) analysis shows harmonics of the gear mesh frequency with varying sideband modulation.

(4). A joint time-frequency analysis (JTFA) during start-up reveals unique vibration patterns when the contact forces increase during acceleration. This research provides a foundation for future vibration-based diagnosis of planetary gears with damaged teeth.

ACKNOWLEDGEMENTS

The authors acknowledge the Donald E. Bently Center for Engineering Innovation at California Polytechnic State University San Luis Obispo for support of this work.

COMPETING INTERESTS

Authors have declared that no competing interests exist.

REFERENCES

1. Lin J, Parker RG. Parametric instability of planetary gears under mesh stiffness variation. Journal of Sound and Vibration. 2002;249:129-145.
2. Lin J, Parker RG. Analytical characterization of the unique properties of planetary gear free vibration. ASME Journal of Vibration and Acoustics, 1999;121:316-321.
3. Guo Yi, Parker RG. Dynamic modeling and analysis of a spur planetary gear involving tooth wedging and bearing clearance nonlinearity. European Journal of Mechanics A/Solids. 2010;29:1022-1033.
4. Parker RG, Wu X. Vibration modes of planetary gears with unequally spaced planets and an elastic ring gear. Journal of Sound and Vibration. 2010;329:2265-2275.
5. Yichao Guo, Parker RG. Purely rotational model and vibration modes of compound planetary gears. Mechanism and Machine Theory. 2010;45:365–377.
6. Kong D, Meagher J, Xu C, Wu X, Wu Y, Nonlinear contact analysis of gear teeth for malfunction diagnostics. IMAC XXVI a Conference on Structural Dynamics, Society for Experimental Mechanics, Orlando, Florida USA, February 4–7; 2008.
7. MSC Inc., MSC ADAMS reference manual.
8. Sommer A, Meagher J, Wu X. Gear defect modeling of a multiple-stage gear train. Modelling and Simulation in Engineering. 2011;2011;8. Article ID 754257.
9. Wu X, Meagher J, Sommer A. A differential planetary gear model with backlash and teeth damage. IMAC XXIX a Conference and Exposition on Structural Dynamics, Society for Experimental Mechanics, Jacksonville, Florida USA; 2011.
10. Yang DCH, Sun ZS. A rotary model for spur gear dynamics. ASME Journal of Mechanisms, Transmissions, and Automation in Design. 1985;107:529–535.
11. Wu X, Fang B, Meagher J, Sommer A. Frequency-domain analysis of a two-stage planetary gear with combined backlash and tooth damage nonlinearities. Proceedings of the ASME 2013 International Design Engineering Technical Conferences & Computers and Information in Engineering Conference, IDETC/CIE 2013, Article Number, DETC2013-13650.
12. Sommer A. Vibration-based health monitoring of multiple-stage gear train and differential planetary transmission involving teeth damage and backlash nonlinearity", September, Master's Thesis, California Polytechnic State University, San Luis Obispo, California, USA; 2011.
13. Fang B, Wu X. Vibration-based health monitoring of damaged bevel gears using ADAMS. Proceedings of 2013 MSC Software Users Conference, May 7-8, Irvine, California, USA; 2013.
14. Wu X, Meagher J, Sommer A. Practical considerations for transient and FFT analyses of planetary gears using ADAMS. Proceedings of MSC Software 2011 Users Conference, October 4-6, Costa Mesa, California; 2011.
15. Sommer A, Meagher J, Wu X. Gear defect modeling of a multiple-stage gear train. Modelling and Simulation in Engineering, 2011;2011:8. Article ID 754257. (Journal Publication).
16. Sommer A, Meagher J, Wu X. An advanced numerical model of gear tooth loading from backlash and profile errors. Proceedings of IMAC XXIX a Conference and Exposition on Structural Dynamics, Society for Experimental Mechanics, Jacksonville, Florida USA; 2011.

Peer-review history:
The peer review history for this paper can be accessed here:
http://sciencedomain.org/review-history/12884